BioEnergy Research (2019) 12:184–196
https://doi.org/10.1007/s12155-018-9955-7

Optimization of Carbonization Process for the Production of Solid Biofuel from Corn Stalk Using Response Surface Methodology

Yajun Wang[1] · Ling Qiu[1,2] · Tianle Zhang[1] · Xuanmin Yang[1,2] · Kang Kang[1]

Published online: 3 January 2019

Abstract

Corn stalk is not suitable for direct combustion due to poor grindability, high moisture content, and insufficient heating value. The aim of this study was to optimize reaction conditions to improve the quality of corn stalk char, and to investigate the effects of carbonization on the physicochemical and combustion characteristics of corn stalks and chars. Optimal conditions for the carbonization of corn stalk were investigated with regard to temperature, holding time, and particle size. Response surface methodology (RSM) provided satisfactory models of responses, and the optimal conditions for higher heating values were obtained as follows: temperature of 551 °C, holding time of 150 min, and particle size range of 0.8–1.0 mm. In addition, after carbonization, changes in surface morphology, functional groups, and organic elements were clearly observed on the chars. The optimal point char experienced fairly complete carbonization, and holds promise for use as a solid biofuel.

Keywords Char · Response surface methodology · Physicochemical properties · Combustion characteristic

Introduction

The overuse of fossil fuels has given rise to various energy and environmental issues, which have driven the need to explore new sources of clean energy. Biomass is an important renewable energy source which stores solar energy and can be converted into various fuels that are carbon-neutral [1]. As an important type of biomass, agricultural waste has long been a focus in the field of renewable energy utilization. In addition to wheat and rice, corn is one of the world's main food crops, especially in China. A total of 215.89 million tons of corn was produced in China in 2017 (data from National Bureau of Statistics of PRC in 2017), and about 270 million tons of corn stalks were also produced in 1 year [2]. Until now, corn stalks have not been used efficiently, and the random burning of corn stalks has caused serious environmental pollution [3, 4]. Therefore, the problem of corn stalk disposal requires urgent attention.

✉ Ling Qiu
xbgzzh@163.com

✉ Kang Kang
kknwafu@hotmail.com

[1] College of Mechanical and Electronic Engineering, Northwest A&F University, Yangling 712100, China

[2] Northwest Research Center of Rural Renewable Energy Exploitation and Utilization, Ministry of Agriculture, Yangling 712100, China

Besides returning to the soil, conversion of this agricultural waste into fertilizer, fodder, base material, and fuel has been reported [5–8]. Unfortunately, the application of corn stalk as a fuel is limited by its poor grindability, high moisture content, and insufficient heat value. Specifically, poor grindability increases the difficulty of biomass formation and pulverization. The moisture in the biomass requires considerable heat for evaporation during drying and combustion, hence reducing the thermal efficiency of the process. In addition, high moisture content and insufficient heat value lead to both increased transportation costs and lower fuel quality [9]. Therefore, pretreatment of corn stalks is necessary to improve their quality as a solid fuel.

As one of the thermochemical conversion routes of biomass, carbonization refers to the process whereby biomass is heated and becomes char after thermal decomposition under anoxic conditions [10]. During carbonization, hydrogen and oxygen are removed due to drying and release of volatile compounds, resulting in the enrichment of carbon in the solid products, and thus improved fuel quality.

Most previous studies have focused on bio-oil characteristics using response surface methodology (RSM) [11–13], and only a few studies have been carried out solely to optimize the fuel quality of solid products and analyze the quality of the optimal sample. Abas et al. [11] optimized the production process of pyrolysis oil from oil palm fiber using RSM via a central composite design (CCD) approach. The effects of

thermochemical catalytic liquefaction conditions including solvent, catalyst, reaction time, temperature, ratio of raw material to solvent, and catalyst dosage were studied via RSM in a study by Li et al. [12]. In addition, Hu et al. [13] applied RSM to evaluate the main and interaction effects of experimental factors on pyrolysis oil and char yields simultaneously. A novelty of the present study is its attempts to determine optimal processes using RSM and to consider char yield, fixed carbon content, higher heating value (HHV), and energy yield as responses. Another contribution of this paper is a more comprehensive comparison of char properties. Fourier transform infrared (FT-IR) spectroscopy, thermogravimetric analysis (TGA), and scanning electron microscopy (SEM) are also used to analyze the change in characteristics during the carbonization process.

Materials and Methods

Materials

Corn stalks were collected from farmland located in Yangling, Shaanxi, China. The samples were screened into different particle size ranges of 0–0.2, 0.2–0.4, 0.4–0.6, 0.6–0.8, and 0.8–1 mm, and then dried for 12 h at 105 ± 5 °C. Proximate analysis of corn stalk with different particle sizes was conducted following ASTM D3173 and D3175 standards to determine their basic physicochemical properties, as shown in Table 1. The HHV of corn stalks and the char samples were determined using a bomb calorimeter (ZDHW-9000, HongKe, China).

Experimental Design

A central composite design (CCD) method was constructed for ordering of the optimization experiments using Design-Expert software, version 8.0.6 (Stat-Ease, Inc., USA). CCD is a type of RSM which was developed in the 1950s [14]. Three experimental factors were selected for this design, namely, temperature, holding time, and particle size. The CCD had star points at a distance of ±1.68 from the central point. The experiments were designed in order to study the influence and determine the optimal values of three factors: char yield, HHV, and energy yield. The experimental setting with reaction conditions and codes are given in Table 2. In total, 20 experiments (6 central points, 6 star points, and 8 factorial points) were required. Except for the central points, each experiment was run three times and the mean was taken to ensure the accuracy of the test. Analysis of variance (ANOVA) was performed on the experimental data, which helped to determine the significance of the results. Based on the various responses, appropriate models were selected to avoid collinearity problems. In addition, optimal carbonization conditions for the highest HHV were identified by the numerical optimization function built into the software.

Carbonization Experiments

All the carbonization experiments were performed in a fixed-bed tube furnace reactor 800 mm in length, with a diameter of 100 mm (SK-G08123K, Zhonghuan, China), as shown in Fig. 1. For each experiment, 6 g of corn stalk was loaded into a porcelain crucible and placed in the center of the quartz tube. A vacuum pump was connected to the tube furnace to remove the air before each experiment. Nitrogen gas was passed through the tube reactor at a flow rate of 20 mL/min for 10 min before the experimental run. The released gas was condensed by a simple heat exchanger before discharge from the system. During the run, the reactor was heated by the electric furnace at a rate of 4 °C/min until the final temperature (200, 300, 450, 600, or 700 °C) was reached. The char yield was calculated by dividing the mass of char after carbonization by the mass of original corn stalk loaded. The HHV yield of char samples was calculated as follows:

$$\text{Energy yield} = \text{char yield} \times \text{HHV of char samples}/\text{HHV of raw materials} \quad (1)$$

Analysis Methods

The raw materials and the samples in central points and optimal points were selected to analyze the physicochemical characteristics. An elemental analyzer (1108CHN, Fisons, USA) was used to detect the content of C, H, N, and O. A scanning

Table 1 Properties of corn stalk with different particle sizes

Analysis	Particle size (mm)				
	0–0.2	0.2–0.4	0.4–0.6	0.6–0.8	0.8–1
Ash content (wt.%)	6.17 ± 0.21	4.48 ± 0.37	3.87 ± 0.22	3.57 ± 0.42	2.61 ± 0.14
Moisture content (wt.%)	9.54 ± 0.37	9.91 ± 0.40	7.91 ± 0.21	9.72 ± 0.17	9.44 ± 0.13
Volatile matter (wt.%)	71.85 ± 0.24	70.15 ± 0.38	73.01 ± 0.09	72.33 ± 0.35	76.61 ± 0.20
Fixed carbon (wt.%)	12.44 ± 0.56	15.46 ± 0.33	15.22 ± 0.27	14.37 ± 0.17	11.34 ± 0.29
Higher heating value (MJ/kg)	15.88 ± 0.17	16.24 ± 0.35	16.35 ± 0.15	16.46 ± 0.08	17.99 ± 0.41

Table 2 Array of the CCD experimental design and the response results

Run	Coded levels			Variables			Response 1	Response 2	Response 3	Response 4
	X1	X2	X3	Temperature (°C)	Holding time (min)	Particle size range (mm)	Char yield (%)	Fixed carbon content (%)	HHV (MJ/kg)	Energy yield (%)
1[b]	0	0	0	450	75	0.4–0.6	29.73	71.28	28.56	51.93
2	−1	−1	1	300	30	0.6–0.8	41.32 ± 0.38	52.77 ± 0.24	27.86 ± 0.25	70.41
3	−1	−1	−1	300	30	0.2–0.4	42.03 ± 0.21	50.12 ± 0.17	26.45 ± 0.21	67.99
4	−1	1	1	300	120	0.6–0.8	39.50 ± 0.48	57.75 ± 0.18	28.56 ± 0.39	69.00
5	0	−1.68	0	450	0[a]	0.4–0.6	31.03 ± 0.25	69.23 ± 0.33	28.45 ± 0.27	53.99
6	0	0	1.68	450	75	0.8–1.0 [a]	30.38 ± 0.12	73.45 ± 0.21	29.60 ± 0.31	55.00
7	1	−1	1	600	30	0.6–0.8	29.19 ± 0.32	77.64 ± 0.30	29.73 ± 0.61	53.08
8	0	1.68	0	450	150[a]	0.4–0.6	29.11 ± 0.19	71.93 ± 0.43	29.77 ± 0.30	53.00
9 [b]	0	0	0	450	75	0.4–0.6	30.08	71.88	28.81	53.00
10	−1	1	−1	300	120	0.2–0.4	38.84 ± 0.38	52.98 ± 0.34	27.78 ± 0.43	65.99
11	1	1	1	600	120	0.6–0.8	28.59 ± 0.42	80.85 ± 0.26	30.39 ± 0.62	53.14
12	0	0	−1.68	450	75	0.0–0.2[a]	33.35 ± 0.37	64.14 ± 0.24	26.96 ± 0.18	54.99
13 [b]	0	0	0	450	75	0.4–0.6	29.20	71.22	28.56	51.01
14	−1.68	0	0	200[a]	75	0.4–0.6	79.26 ± 0.56	18.64 ± 0.31	21.65 ± 0.36	104.95
15	1	−1	−1	600	30	0.2–0.4	29.33 ± 0.45	74.59 ± 0.15	28.99 ± 0.47	52.00
16 [b]	0	0	0	450	75	0.4–0.6	28.88	71.09	28.87	50.99
17 [b]	0	0	0	450	75	0.4–0.6	28.93	70.88	28.82	50.99
18 [b]	0	0	0	450	75	0.4–0.6	29.47	71.23	28.85	52.00
19	1	1	−1	600	120	0.2–0.4	29.21 ± 0.33	79.06 ± 0.12	29.31 ± 0.37	52.36
20	1.68	0	0	700[a]	75	0.4–0.6	27.57 ± 0.58	78.19 ± 0.30	28.36 ± 0.53	47.82

[a] The true values of codes of ±1.68 were set to 200 and 700 °C for temperature, 0 and 150 min for holding time, and 0.0–0.2 and 0.8–1.0 mm for particle size range

[b] The central point experiments were runs 1, 9, 13, 16, 17, and 18. They were repetitive and there were no error data in these experiments

electron microscope (TM3030, Hitachi, Japan) was used for characterizing the surface morphology of the selected samples. Prior to analysis, 1 mg of sample was dried and fixed on an aluminum stub. SEM images were obtained with an incident electron beam at 5 kV at two different magnification ratios. FT-IR analysis was carried out to analyze the changes in the functional groups and was recorded using FT-IR spectroscopy (Nicolet iS10, Thermo Scientific, USA) with a scanned area of 500–4000 cm^{-1}. A thermogravimetric analyzer/differential scanning calorimeter (TGA/DSC,

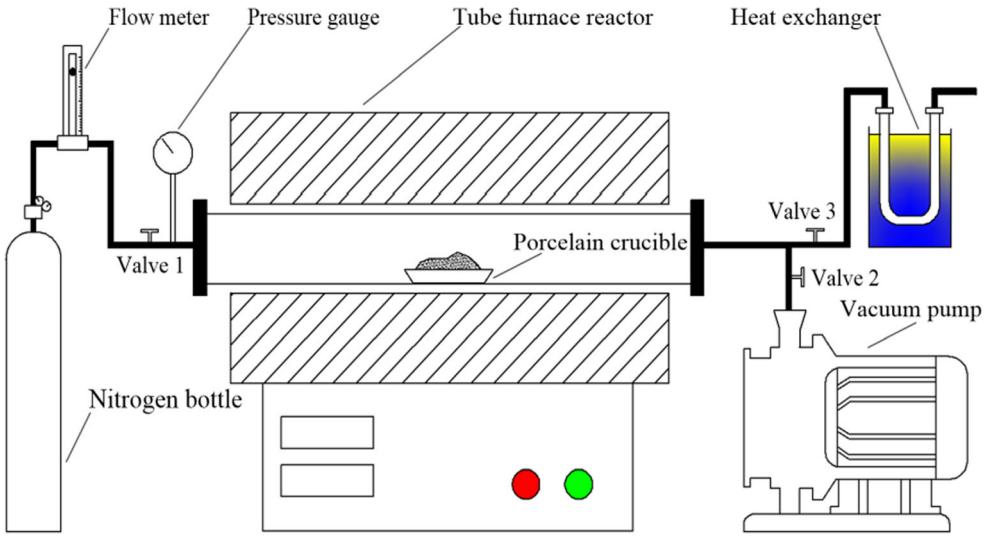

Fig. 1 Schematic of the pyrolysis reactor

METTLER TOLEDO, USA) was employed to evaluate the combustion properties of the samples. Experiments were carried out in an oxygen atmosphere within a temperature range of 40–800 °C at a heating rate of 10 °C/min and an oxygen flux of 20 mL/min.

Results and Discussion

Response Surface Analysis for Char Yield

Char yield and fixed carbon content are critical parameters with regard to char quality. According to the results presented in Table 2, quartic was considered an appropriate process order for char yield. A, B, and C represent temperature (°C), holding time (min), and particle size range (mm), respectively, and the modified regression model for char yield (Y_1) was obtained as follows:

$$Y_1 = 29.32 - 0.17A - 0.58B + 0.52C + 0.66AB + 0.24BC + 2.13A^2 + 0.26B^2 + 0.90C^2 - 5.37A^3 - 0.50C^3 + 2.26A^4 \quad (2)$$

where A = (temperature-450)/150, B = (holding time-75)/45, C = (particle size $_{max}$ - particle size $_{min}$-1)/0.4.

The results of ANOVA for char yield are summarized in Table 3. The results show that the predicted responses using the quartic model are close to the experimental values recorded, with adjusted *R*-squared of 0.99. The lack of fit was not significant, indicating that the model fit was acceptable. The effects of factors on the char yield are shown in Fig. 2 (the effects of the interaction between temperature and holding time and between particle size and holding time are shown in Fig. 2a and b, respectively). It is clear that temperature was the most important factor of the three. With the successive decomposition of hemicellulose, cellulose, and lignin, a massive amount of volatiles were released from the raw materials and caused the mass to decrease [15]. In a study by Park [16], it was found that the decomposition of hemicellulose and cellulose was completed at around 380 °C. At higher temperatures, decomposition of lignin occurs, yielding mainly char. This is also the main reason for the downward trend of the curve in Fig. 2c. The results of elemental analysis showed that the whole carbonization process experienced enrichment of carbon and removal of hydrogen and oxygen [17]. Under a certain temperature, the extension of holding time also showed a negative effect on the char yield (Fig. 2d). A longer holding time could ensure sufficient reaction of samples, especially for the portion with large particles. In addition, some literature has reported that a longer holding time can facilitate the secondary decomposition of solid product to generate non-condensable gas [10, 18, 19].

Generally, due to the lag in heat transfer and incomplete reaction in the large particles, particle size shows a positive effect on char yield in terms of numerical performance [20]. However, as shown in Fig. 2e, this trend was not observed: the curve tended first to fall and then to rise. It was thought that a major portion of the impurities existed in the leaf surface and were retained in the lower particle range with the crushed leaves. Through the proximate analysis in Table 1, the higher ash content of 6.17% in the samples with particle sizes of 0–0.2 mm confirmed this hypothesis. In addition, ash content of 18.60% was observed in the char produced from raw materials with particle size of 0–0.2 mm, while it was 10.81% when the particle size range increased to 0.8–1 mm with the same reaction temperature and holding time (runs 6 and 12 in Table 2). The effect of ash on char yield was also analyzed by Park et al. [21], who noted that the char yields included the contribution of ash that mostly remained in the solid residue. This opinion is in coherence with the results of the current study, indicating that ash is an influential factor that cannot be ignored.

Response Surface Analysis for Fixed Carbon, HHV, and Energy Yield

Most of the carbon in the corn stalks existed in the form of organic matter. Part of the organic matter was released as volatiles and the remaining was converted to fixed carbon [22]. The fixed carbon content obtained from the proximate analysis is important in terms of the quality of the fuel, especially the HHV and energy yield. In this experimental design, fixed carbon, HHV, and energy yield were used as three responses for analyzing the influences of three variables. The effects of the interaction between temperature (A) and holding time (B) and between temperature (A) and particle size range (C) are shown in Fig. 3. The impact of the interaction between B and C was not significant and so is not discussed in detail.

As shown in Fig. 3a and b, it is clear that temperature was the most important factor influencing the fixed carbon content, with a value of Prob > F of less than 0.001, compared to Prob > F values of of 0.1914 and 0.0798 for the holding time and particle size, respectively. The fixed carbon content increased sharply with increasing carbonization temperature, exhibiting a maximum of 80.85% under a reaction temperature of 600 °C, holding time of 120 min, and particle size range of 0.6–0.8 mm (run 11). In addition, runs 19 and 20 showed good performance, producing char with 79.06% and 78.19% fixed carbon content, respectively. Equation (3) plotted in terms of coded levels shows the correlation between reaction conditions and fixed carbon content.

Table 3 Analysis of variance for the adjusted model for the HHV and energy yield of chars

Source	Sum of squares	Degrees of freedom	Mean square	*F* value	*p* value
Char yield (process order: quartic, selection: stepwise)					
Model	2534.55	10	253.46	1405.82	<0.0001
Residual	1.62	9	0.18		
Lack of fit	0.66	4	0.16	0.86	0.5468
Pure error	0.96	5	0.19		
Corrected total	2536.18	19			
R^2: 0.9994					
R^2 adjusted: 0.99					
Fixed carbon (process order: quadratic, selection: manual)					
Model	3773.97	9	419.33	27.94	<0.0001
Residual	150.1	10	15.01		
Lack of fit	149.54	5	29.91	266.79	<0.0001
Pure error	0.56	5	0.11		
Corrected total	3924.08	19			
R^2: 0.9617					
R^2 adjusted: 0.93					
HHV (process order: quadratic, selection: manual)					
Model	54.12	9	6.01	6.74	0.0031
Residual	8.92	10	0.89		
Lack of fit	8.82	5	1.76	84.03	<0.0001
Pure error	0.10	5	0.021		
Corrected total	63.05	19			
R^2: 0.85					
R^2 adjusted: 0.73					
Energy yield (process order: quadratic, selection: manual)					
Model	2881.69	9	320.19	10.96	0.0004
Residual	292.25	10	29.22		
Lack of fit	288.96	5	57.79	87.93	<0.0001
Pure error	3.29	5	0.66		
Corrected total	3173.94	19			
R^2: 0.9079					
R^2 adjusted: 0.83					

$$Y_2 = 71.15 + 14.55A + 1.47B + 2.04C - 0.02AB - 0.32AC + 0.11BC - 7.31A^2 + 0.53B^2 - 0.1C^2 \quad (3)$$

$$Y_3 = 28.70 + 1.4A + 0.38B + 0.62C - 0.13AB - 0.046AC - 0.036BC - 1.06A^2 + 0.39B^2 + 0.099C^2 \quad (4)$$

$$Y_4 = 51.60 - 11.63A - 0.34B + 0.54C + 0.48AB - 0.45AC + 0.036BC + 8.41A^2 + 0.32B^2 + 0.85C^2 \quad (5)$$

where A = (temperature-450)/150, B = (holding time-75)/45, C = (particle size $_{max}$ - particle size $_{min}$-1)/0.4.

HHV is defined as the maximum amount of energy that can be released upon combustion of 1 kg of the sample. Improving the HHV and increasing the energy density are the main purpose of carbonization [23]. Similar to the tendency of fixed carbon, HHV increased with the extent of carbonization. This illustrates that fixed carbon content played a decisive role in HHV. The HHV ranged from 16.35 to 30.39 MJ/kg, implying that the energy content in the treated samples increased by 32–85% as compared to the untreated biomass. HHV was fitted to the response surface model provided by the mathematical models shown in Eq. (4). The *F* value of 6.74 for the model implied that it was significant. A, C, and A^2 were significant model terms, with values of Prob > F at 0.0003, 0.0360, and 0.0017, respectively. Interestingly, regardless of the interactions between A–B or A–C in Fig. 3c and d, both rising trends in HHV stopped at the temperature code levels of 0.5–1 and decreased thereafter. The results show that a high reaction temperature could not guarantee high HHV, and the optimal

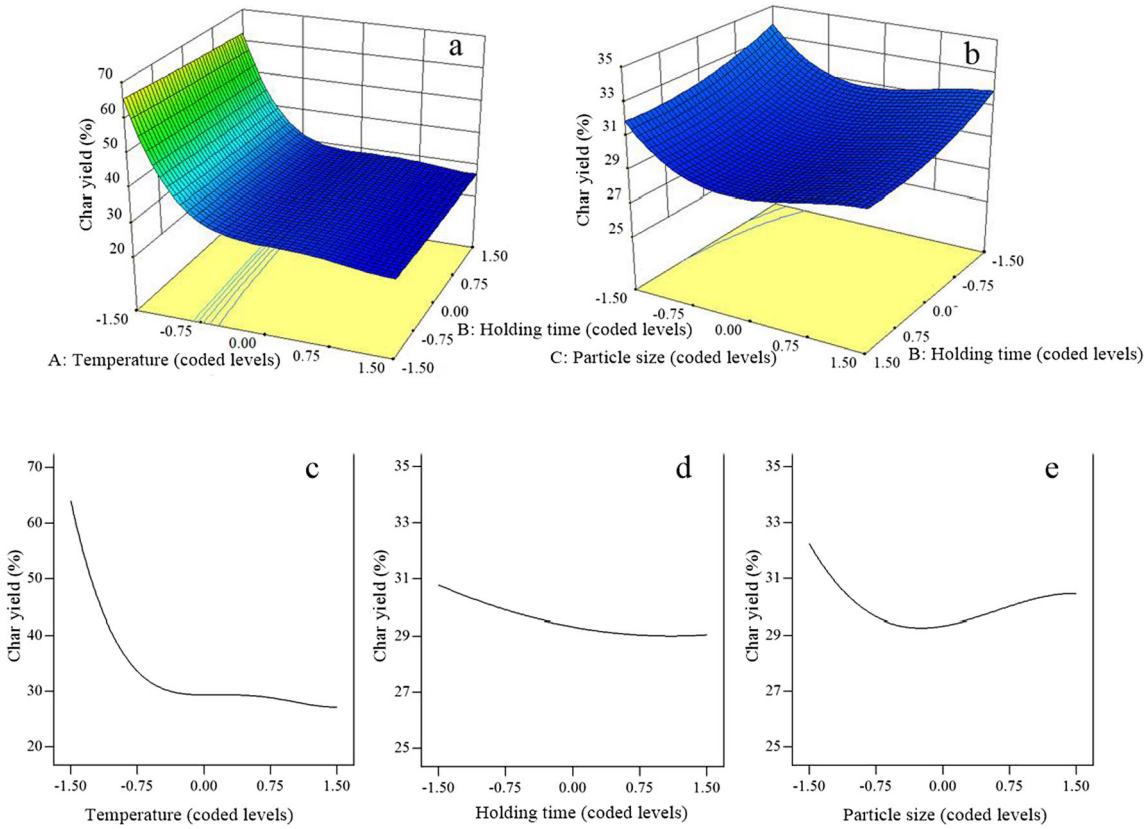

Fig. 2 Effects of factors on char yield: **a** effect of interaction between temperature and holding time on char yield, **b** effect of interaction between particle size and holding time on char yield, **c** effect of temperature, **d** effect of holding time, **e** effect of particle size (the coded level of the factor not appearing was set to 0)

conditions are indicated in the highlighted areas in Fig. 3c and d, respectively. The optimal conditions determined by the optimization function in Design-Expert were a temperature of 551 °C, holding time of 150 min, and particle size range of 0.8–1 mm. The predicted HHV of produced char was 31.93 MJ/kg. A verification experiment was carried out in triplicate, and the average HHV of chars produced under these conditions was 30.78 MJ/kg, a difference of 3.60% from the predicted value. This char sample with a satisfactory HHV was also considered as an optimal point in the following analysis of performance.

The energy yield of chars was calculated using Eq. (1) and represents the extent of the energy conversion of raw materials after carbonization [24]. The results for energy yield in Table 2 ranged from 47.82 (run 20) to 104.95% (run 14). It was found that the quadratic model could provide an appropriate result, with an *R*-squared (R^2) of 0.9079 and adjusted *R*-squared (adjusted R^2) of 0.8251. Equation (5) shows the response surface model of energy yield, which has a *p* value of 0.0004, indicating only a 0.04% chance that a model *F* value this large could occur due to noise. The energy yield results obtained for the chars for all runs are given in Fig. 2e and f. Similar to the trend of the char yield, the energy yield decreased with an increase in temperature, as part of the energy was lost by the release of volatiles. Compared with the other terms, A and A^2 had values for Prob > F of <0.0001 and < 0.0001, respectively, which means that the temperature had a more significant impact on the energy yield.

Analysis of Physicochemical and Combustion Characteristics

The samples of the central point (450 °C, 75 min, 0.4–0.6 mm), the optimal point (551 °C, 150 min, 0.8–1.0 mm), and raw material were selected for comparison.

Char Morphology

A close inspection of raw material and selected char samples was obtained from SEM images, shown in Fig. 4, which revealed the morphological transformations through carbonization. Compact surface structures and a quasi-honeycomb structure were observed in the raw material. However, in the case of the char sample of the central point, Fig. 4b suggests that there were apparent changes in surface morphology. The char sample of the central point seemed rougher and more brittle in structure. In addition, the quasi-honeycomb substance appeared shrunk and broken. Khanna et al. [25]

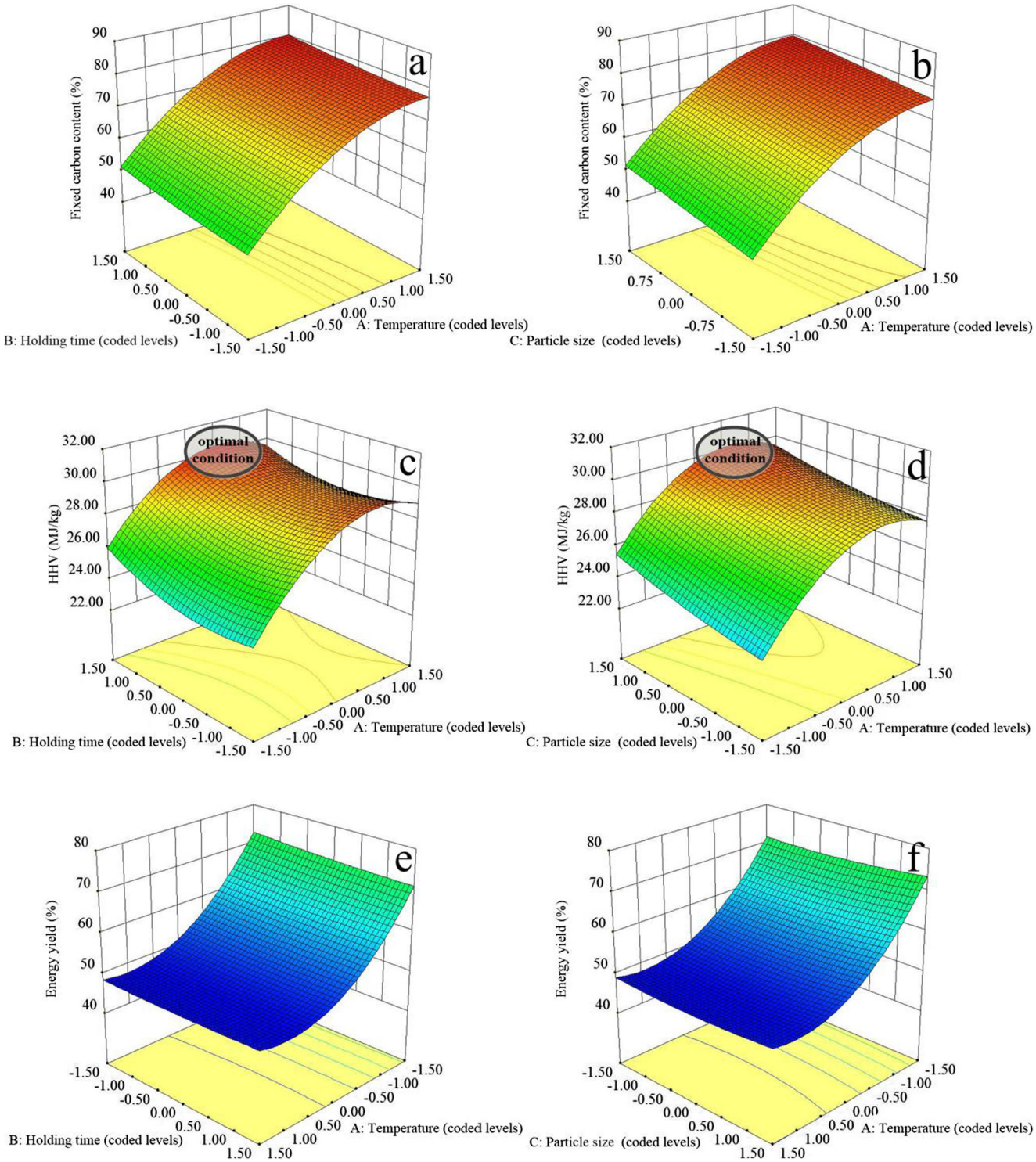

Fig. 3 Effects of interaction **a** between temperature and holding time on fixed carbon content, **b** between temperature and particle size on fixed carbon content, **c** between temperature and holding time on HHV, **d** between temperature and particle size on HHV, **e** between temperature and holding time on energy yield, and **f** between temperature and particle size on energy yield (the coded level of the factor not appearing was set to 0)

concluded that fibers that disappeared at less than 400 °C were associated with cellulose or some of its derivatives, which were regarded as the substance with quasi-honeycomb structure in this study. A similar change was observed on the char sample of the optimal point. The morphological difference was that the pore structure became more clearly defined and the quasi-honeycomb structure almost disappeared. It can be assumed that the thermal treatment applied to the char of the

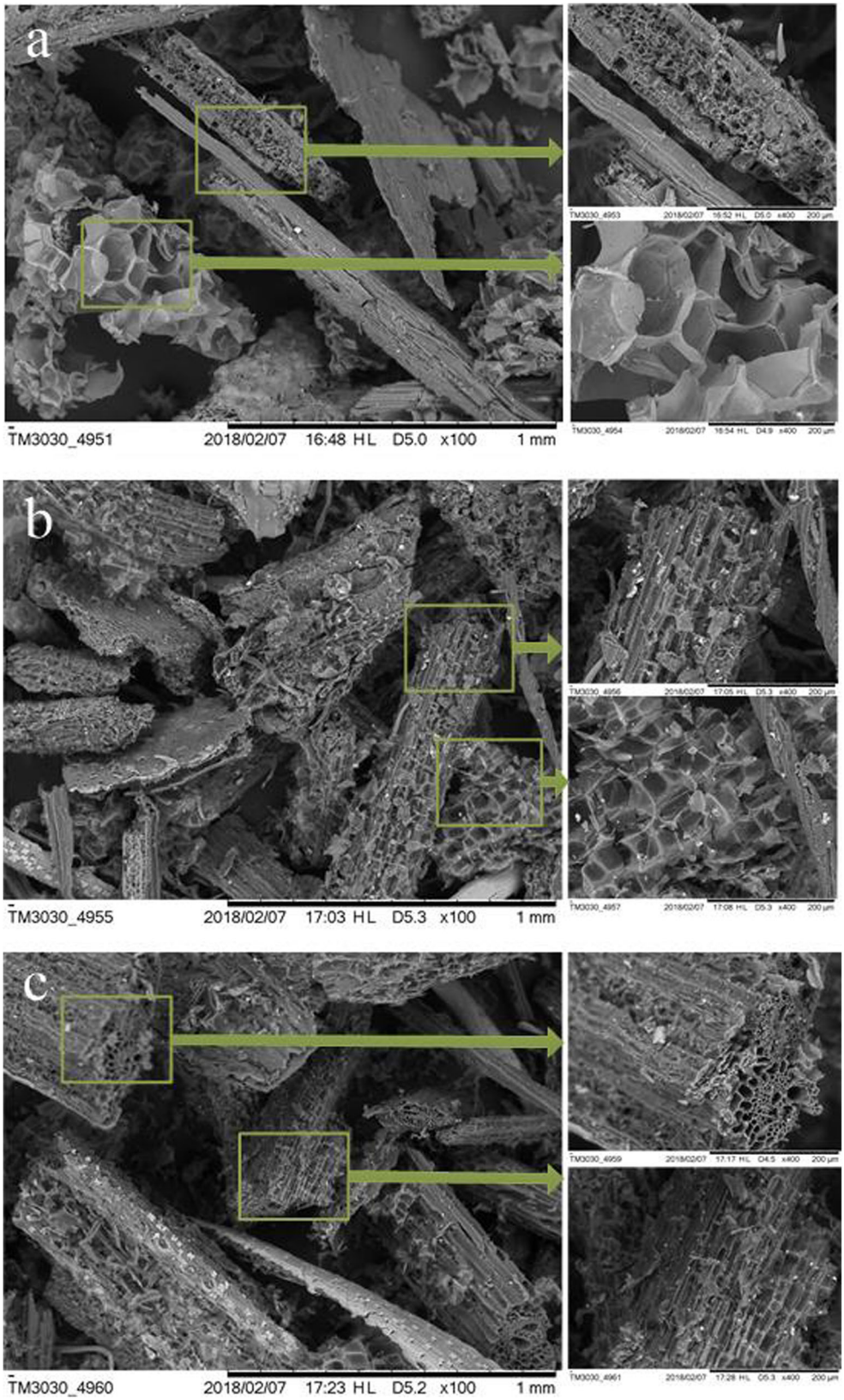

Fig. 4 SEM images of **a** raw materials, **b** char of the central point, **c** char of the optimal point

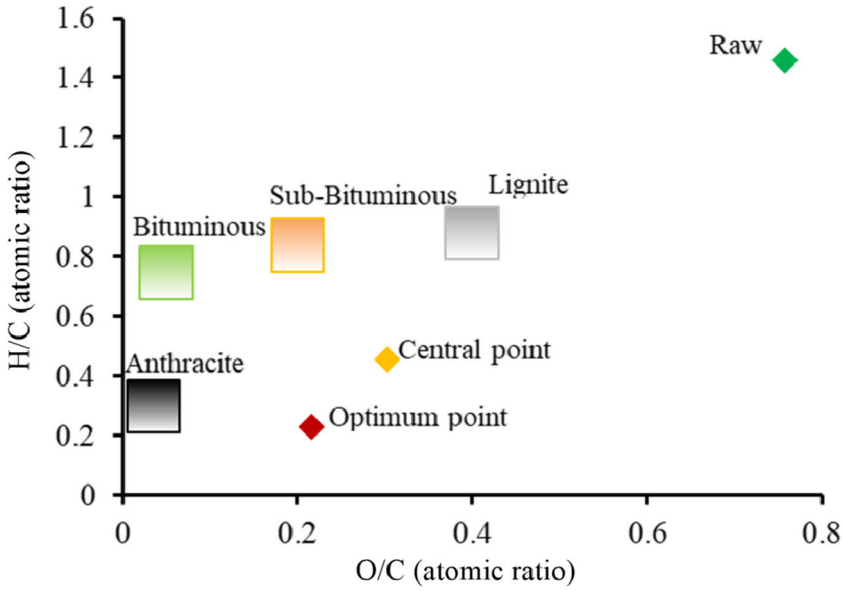

Fig. 5 Van Krevelen diagram for selected samples (anthracite, bituminous, sub-bituminous, and lignite are shown for comparison)

optimal point had a direct influence on the mechanical structure of the solid biofuel. During carbonization, different lignocellulosic components were degraded, with the extent of degradation dependent on the severity of the reaction [26]. The opening of pores in the form of an amorphous and heterogeneous structure resulted from the release of volatile gases from the raw materials [27].

Physicochemical Properties

The Van Krevelen diagram can be used to visualize the carbonization degree of raw materials to chars [28]. Carbonization resulted in higher carbon content and lower oxygen and hydrogen content as the degree of carbonization increased. As shown in Fig. 5, the atomic H/C and O/C ratios of the central point char decreased from 1.46 and 0.76 to 0.46 and 0.30, respectively, and those of the optimal point char decreased to 0.23 and 0.22, respectively. The reduced H/C and O/C atomic ratios indicated the significant effect of carbonization on organic elements due to dehydration and decarboxylation reaction and were linked to an increase in aromaticity [29]. Four typical coals—anthracite, bituminous, sub-bituminous, and lignite—were used to compare the degree of carbonization [30], and the O/C atomic ratios of selected char samples were similar to that of the anthracite. However,

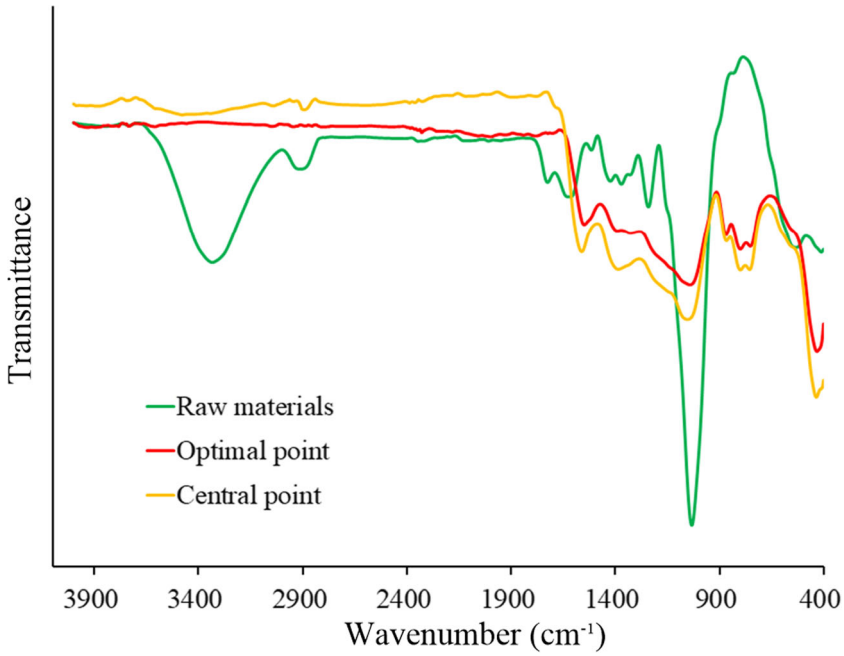

Fig. 6 FT-IR spectra of selected samples

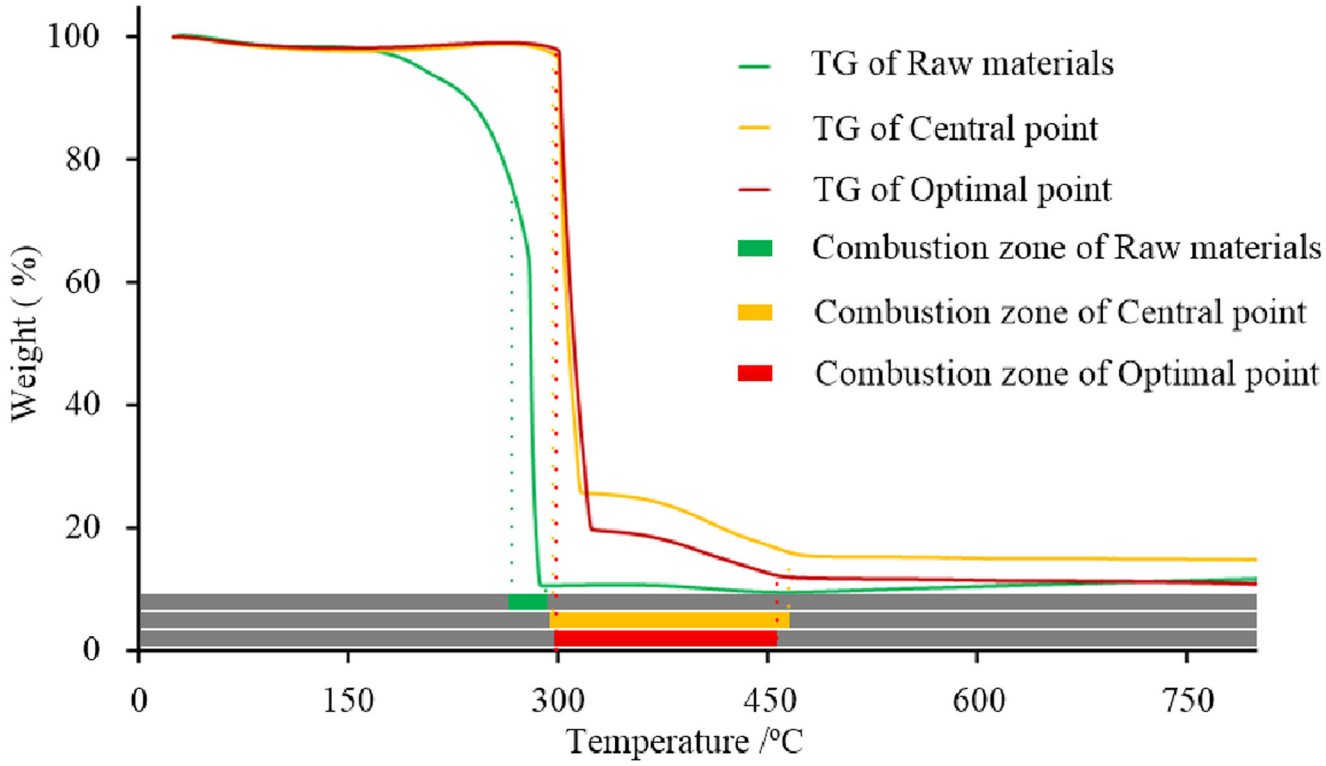

(a)

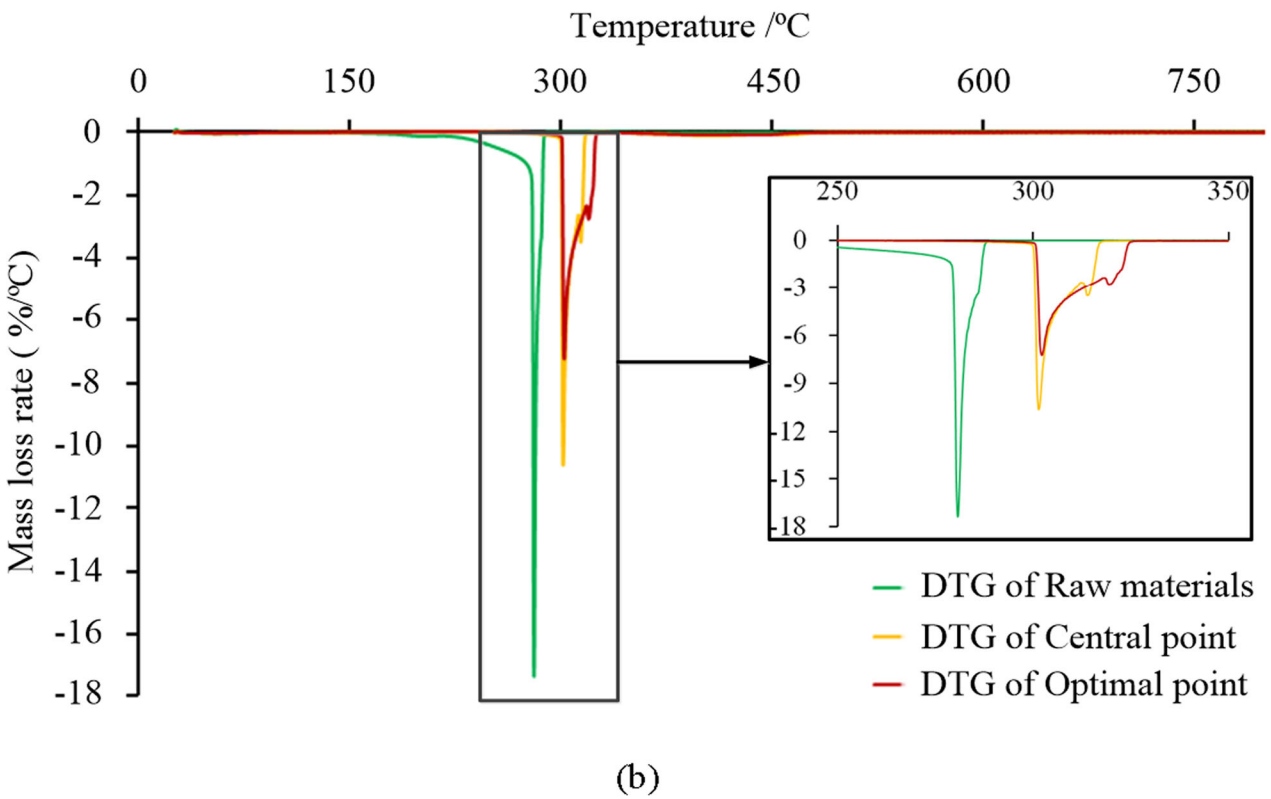

(b)

Fig. 7 TG (**a**) and DTG (**b**) curves of selected samples

the H/C atomic ratios were between sub-bituminous and lignite. This result was similar to other studies that reported a similarity between characteristics of biochar and lignite coal [9, 30, 31]. This demonstrates that selected char samples had satisfactory quality as solid fuel, especially the optimal point char.

To study the structural evolution of the corn stalks during carbonization, FT-IR spectra of selected samples were plotted, and are shown in Fig. 6. It can be observed that the raw materials and treated samples show different spectral patterns. Due to the–OH stretching vibrations, a peak between 3100 and 3600 cm^{-1} can be found in the curve of the corn stalks, and the intensity is decreased in the curves of the two char samples. It was similarly shown that the intensity of peaks between 2800 and 3000 cm^{-1}, which represented the aliphatic groups CH, CH_2, and CH_3, respectively, was decreased in the curves of the latter [32]. These vibrations are expected from hemicellulose, cellulose, and lignin. Compared with raw material, various functional groups were decreased or disappeared between 1000 and 1600 cm^{-1}. For example, the peak around 1370 cm^{-1} represents the C–H stretching and deformation vibrations of cellulose and hemicellulose. With the deepening degree of carbonization, the dehydration and depolymerization of cellulose and hemicellulose caused a decrease in peak strength. Decreased intensity of a peak at 1064 cm^{-1}, which was also ascribed to the β–glycosidic bond in cellulose and hemicellulose, verified a similar conclusion [33]. In addition, new absorption peaks appearing at 755–775 cm^{-1} could be assigned to the C–H group in substituted aryl, which was observed in the samples subjected to higher reaction temperatures.

Analysis of Combustion Characteristics

Figure 7 illustrates the combustion characteristics of selected samples in terms of TG and DTG profiles. As shown in Fig. 7a, on full view of the TG profiles, the differences between the raw materials and the two char samples are obvious. Before burning, the raw materials experienced a period of mass loss as the temperature increased from 200 to 275 °C, while the mass loss of the two char samples was not significant, indicating that the moisture was removed and a portion of hemicellulose was degraded in this temperature range, and the char samples had better hydrophobic performance. This is consistent with the results of FT-IR analysis, where the peak between 3100 and 3600 cm^{-1} was assigned to –OH stretching vibrations. The ignition points were determined using TG-DTG curves based on the method reported by Zhao et al. [34]. The combustion zones were defined as the temperature ranges of the combustion process of selected samples. An ignition point of 276 °C and combustion zone between 276 and 286 °C was found for the raw materials. Char samples of the central point and the optimal point had similar combustion behavior: they were both ignited at 299 °C, and their combustion times were 7.90 min (299–457 °C) and 7.54 min (299–450 °C), respectively. These results suggest that the combustion of char samples shifted to higher temperature ranges with a wider combustion zone compared to the raw materials. The maximum weight loss rates and corresponding temperatures are presented on the DTG profiles (Fig. 7b), and are expressed as $(dw/dT)_{max}$ and T_{max}, respectively. The magnified view shows that the char of the optimal point had $(dw/dT)_{max}$ of −7.23%/°C and T_{max} of 302 °C. The wider combustion zone and decreased maximum weight loss rates indicate that the optimal point char combusted more moderately than the corn stalks [35]. The elevated ignition points coupled with significantly widened combustion zone suggests that higher thermal efficiency can be achieved for the combustion of char samples of the optimal point [36]. This performance may be attributed to the deepening degree of carbonization.

Conclusion

The optimal conditions for carbonization of corn stalks were confirmed with regard to temperature, holding time, and particle size. The results showed that reaction temperature had a strong impact on the HHV and energy yield, while the effects of holding time and particle size were less significant. The statistical models were constructed for char yield, fixed carbon content, HHV, and energy yield, and the fitting of equations showed satisfactory results. In addition, the optimal conditions for HHV were a temperature of 551 °C, holding time of 150 min, and particle size range of 0.8–1 mm. The predicted highest HHV of produced char was 31.93 MJ/kg. Compared with raw materials, the optimal point char showed properties similar to high-quality coal. The results of FT-IR, SEM, and TG-DTG analyses indicated that complete carbonization occurred during the formation of the char at the optimal point.

Acknowledgments This work was supported by the Special Fund for Agro-scientific Research in the Public Interest [No. 201503135] and the Special Rural Energy Science and Technology Project of the Ministry of Agriculture [No. 09172130126249100 3].

References

1. Kang K, Qiu L, Zhu M, Sun G, Wang Y, Sun R (2018) Codensification of agroforestry residue with bio-oil for improved fuel pellets. Energy Fuel 32(1):598–606. https://doi.org/10.1021/acs.energyfuels.7b03482
2. Guo J, Cui X, Sun H, Zhao Q, Wen X, Pang C, Dong R (2018) Effect of glucose and cellulase addition on wet-storage of excessively wilted

maize Stover and biogas production. Bioresour Technol 259:198–206. https://doi.org/10.1016/j.biortech.2018.03.041
3. Biswas B, Pandey N, Bisht Y, Singh R, Kumar J, Bhaskar T (2017) Pyrolysis of agricultural biomass residues: comparative study of corn cob, wheat straw, rice straw and rice husk. Bioresour Technol 237:57–63. https://doi.org/10.1016/j.biortech.2017.02.046
4. Salema AA, Afzal MT, Bennamoun L (2017) Pyrolysis of corn stalk biomass briquettes in a scaled-up microwave technology. Bioresour Technol 233:353–362. https://doi.org/10.1016/j.biortech.2017.02.113
5. Bera T, Purakayastha TJ, Patra AK, Datta SC (2018) Comparative analysis of physicochemical, nutrient, and spectral properties of agricultural residue biochars as influenced by pyrolysis temperatures. J Mater Cycles Waste Manage 20(2):1115–1127. https://doi.org/10.1007/s10163-017-0675-4
6. Soufizadeh M, Pirmohammadi R, Alijoo Y, Behroozyar HK (2018) Indigestible neutral detergent fibers: relationship between forage fragility and neutral detergent fibers digestibility in total mixed ration and some feedstuffs in dairy cattle. Vet Res Forum 9(1):49–57
7. He X, Zhang K, Wang W, Li H, Yin Q (2018) Thermal stability and bonding mechanisms of corn stalk rind. Bioresources 13(2):2748–2758. https://doi.org/10.15376/biores.13.2.2748-2758
8. Wang Q, Han K, Wang J, Gao J, Lu C (2017) Influence of phosphorous based additives on ash melting characteristics during combustion of biomass briquette fuel. Renew Energy 113:428–437. https://doi.org/10.1016/j.renene.2017.06.018
9. Liu Z, Han G (2015) Production of solid fuel biochar from waste biomass by low temperature pyrolysis. Fuel 158:159–165. https://doi.org/10.1016/j.fuel.2015.05.032
10. Wang X, Zhai M, Wang Z, Dong P, Lv W, Liu R (2018) Carbonization and combustion characteristics of palm fiber. Fuel 227:21–26. https://doi.org/10.1016/j.fuel.2018.04.088
11. Abas FZ, Ani FN, Zakaria ZA (2018) Microwave-assisted production of optimized pyrolysis liquid oil from oil palm fiber. J Clean Prod 182:404–413. https://doi.org/10.1016/j.jclepro.2018.02.052
12. Li F, Hu Z, Xiao B (2017) Bio-oil production by thermochemical catalytic liquefaction of bloom-forming cyanobacteria: optimization using response surface methodology (RSM). Energy Fuel 31(12):13733–13742. https://doi.org/10.1021/acs.energyfuels.7b02595
13. Hu G, Li J, Zhang X, Li Y (2017) Investigation of waste biomass co-pyrolysis with petroleum sludge using a response surface methodology. J Environ Manag 192:234–242. https://doi.org/10.1016/j.jenvman.2017.01.069
14. Nam H, Capareda S (2015) Experimental investigation of torrefaction of two agricultural wastes of different composition using RSM (response surface methodology). Energy 91:507–516. https://doi.org/10.1016/j.energy.2015.08.064
15. Li K, Zhu C, Zhang L, Zhu X (2016) Study on pyrolysis characteristics of lignocellulosic biomass impregnated with ammonia source. Bioresour Technol 209:142–147. https://doi.org/10.1016/j.biortech.2016.02.136
16. Park Y-K, Yoo ML, Lee HW, Park SH, Jung S-C, Park S-S, Kim S-C (2012) Effects of operation conditions on pyrolysis characteristics of agricultural residues. Renew Energy 42:125–130. https://doi.org/10.1016/j.renene.2011.08.050
17. Kim D, Lee K, Park KY (2014) Hydrothermal carbonization of anaerobically digested sludge for solid fuel production and energy recovery. Fuel 130:120–125. https://doi.org/10.1016/j.fuel.2014.04.030
18. Pinkowska H, Wolak P (2013) Hydrothermal decomposition of rapeseed straw in subcritical water. Proposal of three-step treatment. Fuel 113:340–346. https://doi.org/10.1016/j.fuel.2013.05.088
19. Peng WM, Wu QY, Tu PG (2000) Effects of temperature and holding time on production of renewable fuels from pyrolysis of Chlorella protothecoides. J Appl Phycol 12(2):147–152. https://doi.org/10.1023/a:1008115025002
20. Suriapparao DV, Vinu R (2018) Effects of biomass particle size on slow pyrolysis kinetics and fast pyrolysis product distribution. Waste Biomass Valoriz 9(3):465–477. https://doi.org/10.1007/s12649-016-9815-7
21. Park J, Lee Y, Ryu C, Park Y-K (2014) Slow pyrolysis of rice straw: analysis of products properties, carbon and energy yields. Bioresour Technol 155:63–70. https://doi.org/10.1016/j.biortech.2013.12.084
22. Ronsse F, van Hecke S, Dickinson D, Prins W (2013) Production and characterization of slow pyrolysis biochar: influence of feedstock type and pyrolysis conditions. Glob Change Biol Bioenergy 5(2):104–115. https://doi.org/10.1111/gcbb.12018
23. Chin KL, H'ng PS, Go WZ, Wong WZ, Lim TW, Maminski M, Paridah MT, Luqman AC (2013) Optimization of torrefaction conditions for high energy density solid biofuel from oil palm biomass and fast growing species available in Malaysia. Ind Crop Prod 49:768–774. https://doi.org/10.1016/j.indcrop.2013.06.007
24. Ianez-Rodriguez I, Angeles Martin-Lara M, Blazquez G, Perez A, Calero M (2017) Effect of torrefaction conditions on greenhouse crop residue: optimization of conditions to upgrade solid characteristics. Bioresour Technol 244:741–749. https://doi.org/10.1016/j.biortech.2017.08.031
25. Khanna R, Ikram-Ul-Haq M, Rajarao R, Cayumil R, Rawal A, Sahajwalla V, Mukherjee PS (2017) Novel multidimensional carbons from structural transformations of waste lignin: a low temperature pyrolysis investigation. Fuel Process Technol 166:312–321. https://doi.org/10.1016/j.fuproc.2017.06.013
26. McNamee P, Darvell LI, Jones JM, Williams A (2015) The combustion characteristics of high-heating-rate chars from untreated and torrefied biomass fuels. Biomass Bioenergy 82:63–72. https://doi.org/10.1016/j.biombioe.2015.05.016
27. Pehlivan E, Ozbay N, Yargic AS, Sahin RZ (2017) Production and characterization of chars from cherry pulp via pyrolysis. J Environ Manag 203:1017–1025. https://doi.org/10.1016/j.jenvman.2017.05.002
28. Peng C, Zhai Y, Zhu Y, Xu B, Wang T, Li C, Zeng G (2016) Production of char from sewage sludge employing hydrothermal carbonization: char properties, combustion behavior and thermal characteristics. Fuel 176:110–118. https://doi.org/10.1016/j.fuel.2016.02.068
29. Anupam K, Sharma AK, Lal PS, Dutta S, Maity S (2016) Preparation, characterization and optimization for upgrading Leucaena leucocephala bark to biochar fuel with high energy yielding. Energy 106:743–756. https://doi.org/10.1016/j.energy.2016.03.100
30. Pala M, Kantarli IC, Buyukisik HB, Yanik J (2014) Hydrothermal carbonization and torrefaction of grape pomace: a comparative evaluation. Bioresour Technol 161:255–262. https://doi.org/10.1016/j.biortech.2014.03.052
31. Wilk M, Magdziarz A, Kalemba I, Gara P (2016) Carbonisation of wood residue into charcoal during low temperature process. Renew Energy 85:507–513. https://doi.org/10.1016/j.renene.2015.06.072
32. Naik S, Goud VV, Rout PK, Jacobson K, Dalai AK (2010) Characterization of Canadian biomass for alternative renewable biofuel. Renew Energy 35(8):1624–1631. https://doi.org/10.1016/j.renene.2009.08.033
33. Liu Z, Balasubramanian R (2014) Upgrading of waste biomass by hydrothermal carbonization (HTC) and low temperature pyrolysis (LTP): a comparative evaluation. Appl Energy 114:857–864. https://doi.org/10.1016/j.apenergy.2013.06.027
34. Zhao P, Ge S, Yoshikawa K (2013) An orthogonal experimental study on solid fuel production from sewage sludge by employing steam explosion. Appl Energy 112:1213–1221. https://doi.org/10.1016/j.apenergy.2013.02.026

35. Liu Z, Quek A, Balasubramanian R (2014) Preparation and characterization of fuel pellets from woody biomass, agro-residues and their corresponding hydrochars. Appl Energy 113:1315–1322. https://doi.org/10.1016/j.apenergy.2013.08.087

36. Obernberger I, Thek G (2004) Physical characterisation and chemical composition of densified biomass fuels with regard to their combustion behaviour. Biomass Bioenergy 27(6):653–669. https://doi.org/10.1016/j.biombioe.2003.07.006